Sources of light particles from fusion-like processes in the $^{20}Ne+^{27}Al$ reaction at 19.2 MeV/nucleon

K. A. Griffioen, E. A. Bakkum, P. Decowski,* R. J. Meijer, and R. Kamermans
Fysisch Laboratorium, Rijksuniversiteit Utrecht, 3508 TA Utrecht, The Netherlands
(Received 2 November 1987)

We have measured light-particle energy spectra over a 90° range of angles in the forward hemisphere in coincidence with heavy residues from the reaction $^{20}Ne+^{27}Al$ at 19.2 MeV/nucleon. A selection on residues with $Z \geq 11$ removes the contributions of deep-inelastic scattering and peripheral processes from the fusion-like cross section. With the help of a simple analytic model that includes the coincidence kinematics we are able to describe the data and extract multiplicities, primary-energy distributions, and source velocities for the light particles from fusion-like reactions. The mass difference between the observed fragments and the compound system comes almost exclusively from light particles with $Z \leq 2$. The evaporated α particles are more energetic and more numerous than the statistical model implies. The fast α particles have distributions consistent with a fragmentation-fusion picture; however, they account for at most $\frac{1}{3}$ of the momentum lost in the incomplete fusion process.

I. INTRODUCTION

Much of the evidence for incomplete fusion (ICF) in nuclear reactions has come from the observation of a shift in the inclusive heavy-residue (HR) velocity distributions away from the velocity expected for a completely fused system.[1] This momentum deficit, however, can only be observed in asymmetric systems for which the escaping momentum comes predominantly from the lighter reaction partner. Incomplete fusion can be described in general terms as an inability of the mean field of the colliding system to fully capture all nucleons with large center-of-mass momenta. This loss is tempered by the effective viscosity of the nuclear medium, i.e., through nucleon-nucleon collisions.[2] Despite fairly good agreement between the momentum deficits predicted by this simple theory and the available data, the precise mechanism for ICF is still not understood. One of the interesting questions at this point is whether the incomplete momentum transfer results from nucleon emission (Fermi jets,[3] promptly emitted particles,[4] preequilibrium emission,[5] etc.) or from heavier particles (massive transfer,[6] breakup-fusion,[7] etc.)

Results from the reaction $^{40}Ar + ^{12}C$ indicate that, at least for a light nucleus like carbon at low energies governed by optimum Q values, ICF comes from cluster transfer of one, two, or three α particles to the argon projectile.[8] Recent experiments on the system $^{14}N + ^{159}Tb$ show a large component of forward-peaked α particles concentrated at energies between the Coulomb barrier and the beam velocity.[9] A coincidence experiment on $^{16}O + ^{27}Al$ similar to our own showed no distinct peak of α particles from fusion near the beam velocity. However, using a statistical-model calculation of the evaporation spectra, these authors proceeded to extract a forward-peaked ICF component from α emission that accounts for most of the momentum deficit.[10] On the other hand, for central collisions with heavy targets a large preequilibrium neutron component is present.[11] The interplay between fast α and nucleon emission in fairly (but not extremely) light systems like $^{20}Ne + ^{27}Al$ should indicate the relative importance of the breakup and the jetting processes.

For beam energies between 10 and 30 MeV/nucleon, where incomplete fusion can be observed, the fused systems that form are highly excited. The resulting evaporation-residue spectra (though shifted in mean velocity from the value expected for full momentum transfer) are broadly distributed in mass, charge and velocity; this makes a separation into complete and incomplete fusion components quite difficult since these broad structures lie on top of each other. Moreover, it is entirely possible that the momentum loss comes not from a single preequilibrium particle, but from a number of them. In this case, it would be more advantageous to talk about a preequilibrium particle multiplicity distribution. To investigate these problems experimentally, we must detect the light particles (LP's) emitted in the reaction. This is not enough, however, since singles LP spectra contain large contributions from peripheral processes that obscure the fusion-like LP spectra. To avoid this difficulty one must turn to experiments that detect heavy residues (these indicate the nature of the reaction) in coincidence with LP's. This technique, as we shall see in the following sections, removes the peripheral contributions to the LP spectra, but creates a kinematic bias. The precise form of the coincidence LP spectra depends on the shape of the HR spectra as well as on the angle at which the HR's are measured. These effects, however, can be calculated and corrected for.

II. EXPERIMENTAL SETUP

The aim of the present experiments was to study incomplete fusion in a fairly light system for which the systematics of the inclusive measurements are already well

known. We have measured coincidences between light particles (p, d, t, ^{3}He, and α) and HR's in the reaction ^{20}Ne + ^{27}Al at 19.2 MeV/nucleon using the cyclotron at KVI in Groningen. Figure 1 shows schematically the detector arrangement. We placed a small freon-filled ionization chamber at 5° with respect to the beam. The back of the ionization chamber contained a 500 μm silicon detector which stopped all beam-velocity particles with charge $Z \geq 8$ and defined the solid angle to be 1.21 msr. The angle 5° is a reasonable compromise between maximal HR counting rates and minimal contributions from peripheral processes which peak at the grazing angle $\theta_g = 3.6°$. Four triple-element LP telescopes complemented the ionization chamber. Telescope D at negative angles (angles on the opposite side of the beam from the ionization chamber) consisted of a position-sensitive silicon detector (8×22 mm$^2 \times 300$ μm) followed by a second silicon detector (500 μm) and a CsI crystal ($3 \times 3 \times 1$ cm^3) with two photodiode light collectors.[12] This telescope was divided into four sections of 1.18 msr each during the analysis. For this experiment, in which 1 MeV resolution is sufficient, the durable and dense (4.51 g/cm^2) CsI crystal is superior to silicon detectors, since it could stop 100 MeV protons and 400 MeV α particles. The telescopes A, B, and C (2.1, 3.3, and 9.3 msr, respectively) consisted of standard silicon detectors in the combination ($\sim$15–100–5000 μm); these were only able to stop 30 MeV protons and 120 MeV α particles. Initially the four telescopes A–D stood at 15°, 35°, 55°, and −24°, respectively. Half way through the measurement we rotated them by 10°; this produced a total of 14 angles spread over a range of 90° in the forward hemisphere. We also measured singles HR spectra in separate runs during the same experiment. The integrated current from a Faraday cup and the measured ^{27}Al target thickness of 540 μg/cm^2 served to normalize the data. We have divided all coincidence LP spectra by the singles HR cross sections in order to eliminate any systematic errors due to the Faraday cup and the target thickness, and to generate differential multiplicities which, when integrated, give the total LP multiplicities.

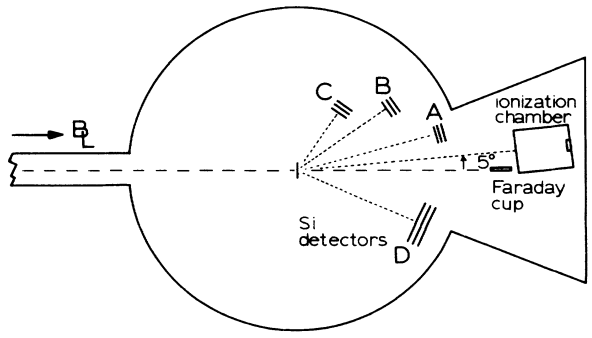

FIG. 1. Detector arrangement. Telescopes A–C are three-element Si detectors. Telescope D consists of a position-sensitive Si detector followed by second Si detector and a CsI crystal.

III. DATA

A. Selecting fusion-like events

Without a selection of fusion-like events, the sequential decay from peripheral processes would dominate the LP spectra (especially near the beam energy where preequilibrium particles from ICF may be present), and make conclusions difficult if not impossible. We must therefore first use the singles heavy-ion spectra to learn what processes are present as a function of HR charge Z, and then make a selection on Z which includes only fusion-like processes. From singles experiments that resolve both mass A and charge Z,[13] one can extract the width σ, the centroid velocity v_0, and the cross section for evaporation residues using the form[14]

$$\frac{d^2\sigma}{dv_H d\Omega_H} = N v_H^2 e^{-(v_H - v_0 \cos\theta_H)^2/2\sigma^2} . \quad (1)$$

Here v_H is the heavy residue velocity measured at lab angle θ_H. For 20 MeV/nucleon ^{20}Ne + ^{27}Al the widths of the evaporation residue (ER) distributions vary smoothly with the residue charge Z as follows:

$$\sigma(Z) = 1.895 - 0.177\,287Z + 0.004\,839Z^2 . \quad (2)$$

When Eq. (1) is transformed to energy variables it takes the form

$$\frac{d^2\sigma}{dE_H d\Omega_H} = N \left[\frac{2E_H}{m^3} \right]^{1/2} e^{-(\sqrt{E_H} - \sqrt{E_0}\cos\theta_H)^2/m\sigma^2} , \quad (3)$$

where $E_0 = \frac{1}{2} m v_0^2$ and m is the residue mass. From the singles data[13] we can also extract the average mass $\overline{A}$ as a function of residue charge:

$$\overline{A}(Z) = 2.053Z + 0.001\,553Z^2 . \quad (4)$$

Although experimentally the source velocity v_0 in Eq. (1) remains nearly constant for different isotopes, the source energy E_0 of Eq. (3) changes quite dramatically due to the changing value of m. This has the effect of broadening the energy spectra for data summed over all masses of a given element.

Assuming that the additional width is proportional to the difference in E_0 for two adjacent masses, we find that this width is proportional to v_0^2. Hence, we can replace Eq. (3) by

$$\frac{d^2\sigma}{dE_H d\Omega_H} = N \left[\frac{2E_H}{\overline{m}^3} \right]^{1/2} e^{-(\sqrt{E_H} - \sqrt{\overline{E}_0}\cos\theta_H)^2/(\overline{m}\sigma^2 + \beta v_0^2)} , \quad (5)$$

where $\overline{m}$ and $\overline{E}_0$ are the average mass and central energy for all isotopes of a given element. We have fit the spectra for $Z = 13$, 14, and 15 with Eq. (5) and deduced the value $\beta v_0^2 = 5.2$ MeV. Using Eqs. (2), (4), and (5) we can estimate the contribution of fusion to the measured α–HR coincidence spectra. Figure 2 shows the heavy-residue spectra for $Z = 9$ to 15 in coincidence with an α particle in any of the light-particle telescopes. These spectra show the prominence of fusion-like processes for

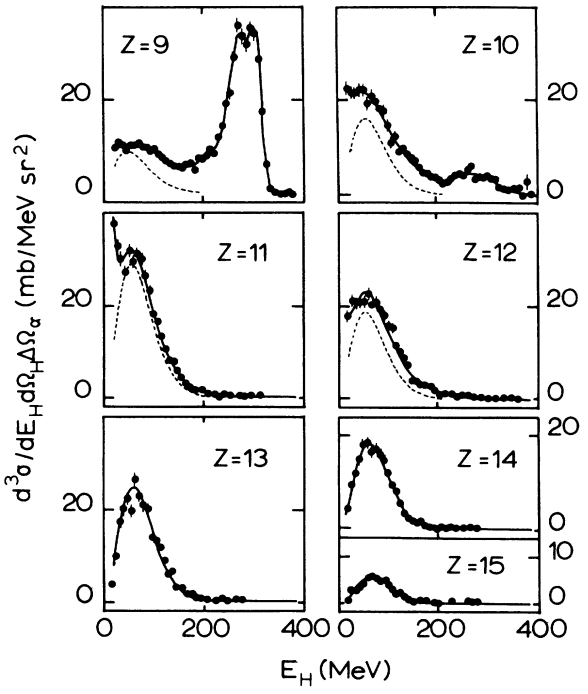

FIG. 2. Heavy residues detected at 5° in coincidence with an α particle in any of the LP detectors. Presented are triply-differential cross section vs heavy-ion energy. The dashed lines are the estimated contribution from fusion (see text).

$Z \geq 11$, and the overwhelming presence of peripheral processes for $Z < 10$. We have fit these data with a fusion component [Eq. (5) with all parameters fixed except for the magnitude] and four components of the form of Eq. (3): one for target recoils with $E_0 = 0$, one for deep inelastic scattering with E_0 near the Coulomb energy, and two with E_0 near the energy of beam-velocity particles. The solid lines in Fig. 2 show the full fit, whereas the dashed lines give the fusion-like component. Table I lists the integrated counts for each component in such a decomposition. Without a full singles angular distribution, one must consider these values as trends rather than exact determinations. However, for the purpose of convincing ourselves that residues with $Z \geq 11$ are predominantly a result of fusion-like processes, these numbers serve very well. The targetlike component present in the $Z = 11, 12$ spectra can easily be removed by a low-energy threshold. Hence, we estimate that at least 88% of the events analyzed with $Z \geq 11$ comes from fusion-like processes. Moreover, these residues account for about 75% of the total fusion-like cross section.

TABLE I. Estimates of various reaction components as a function of Z. The quoted values are integrated counts at $\theta_H = 5°$.

Z	Fusion	Target	Deep inelastic	Peripheral
9	773	216	416	2818
10	1419	535	966	333
11	1590	419	726	0
12	2432	1428	406	0
13	2051	0	0	0
14	1514	0	0	0
15	464	0	0	0
≥ 16	259	0	0	0

B. The coincidence spectra

Given that nearly all residues with $Z \geq 11$ come from complete as well as incomplete fusion, we can select these ions and look at the resulting light-particle spectra. The LP energy spectra can be transformed easily to velocity-invariant cross sections $d^3\sigma/d^3v_L$ and the contours of such plotted as a function of the lab velocities perpendicular and parallel to the beam direction. Figure 3 shows the resulting contour plot for α particles in coincidence with fusion residues at $\theta_H = 5°$. This plot displays 3 interesting regions. Region 2 contains a maximum that is slightly off center and considerably below the beam velocity. Region 1 displays a minimum near the beam axis at the compound nuclear velocity. This minimum results from the fact that the Coulomb barrier for α emission in these systems is fairly high. In region 3 one sees a strong increase in the cross section at small lab velocities. Contrary to the models for incomplete fusion which predict a large component at the beam velocity, (for 20 MeV/nucleon one might expect ~ 1 beam-velocity α particle per reaction) we see no distinct peak at these velocities. Moreover, the large peak (region 2) lies precisely at

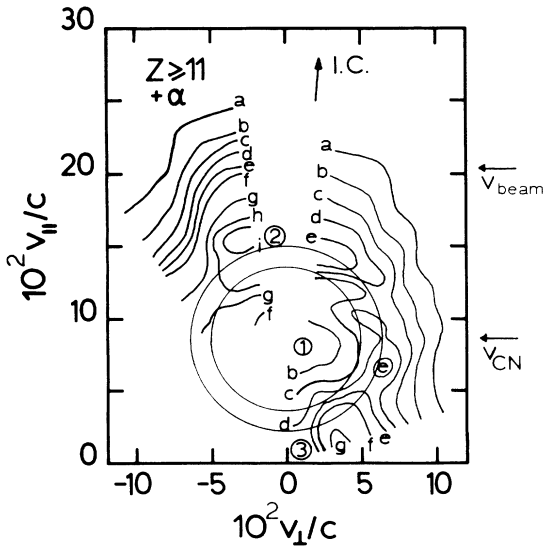

FIG. 3. The invariant velocity contours for α particles in coincidence with heavy residues at 5° with $Z \geq 11$. The inner (outer) circle corresponds to the Coulomb velocity of an α particle emitted from a $Z = 15$ ($Z = 23$) system moving with velocity v_{CN}. The contours, labeled a through i, correspond to 5, 10, 15, 20, 25, 30, 40, 50, and 60×10^4 mb sr^{-1} c^{-3}.

the Coulomb velocity for the $^{43}Sc + \alpha$ system (outer circle). This suggests that most of the α particles that we see come from a nearly, if not completely, equilibrated system.

In contrast, Fig. 4 shows the α particles contours for coincidences with $Z = 8$ nuclei. Here the overwhelming contribution to the light-particle spectrum comes from the sequential decay of inelastic excited ^{20}Ne traveling at nearly the beam velocity. The coincidence kinematics strongly favors the detection of α particles on the opposite side of the beam from the ionization chamber.

Figure 5 shows the proton contours for coincidences with $Z \geq 11$ residues. Again the concentration of cross section lies between the circles corresponding to the Coulomb velocity for $^{46}Ti + p$ and $^{28}Si + p$. The proton spectra show many of the same features as the α data. Likewise, the plots for d, t, and ^3He are similar, with concentrations of cross section along circles corresponding to emission at the Coulomb velocity.

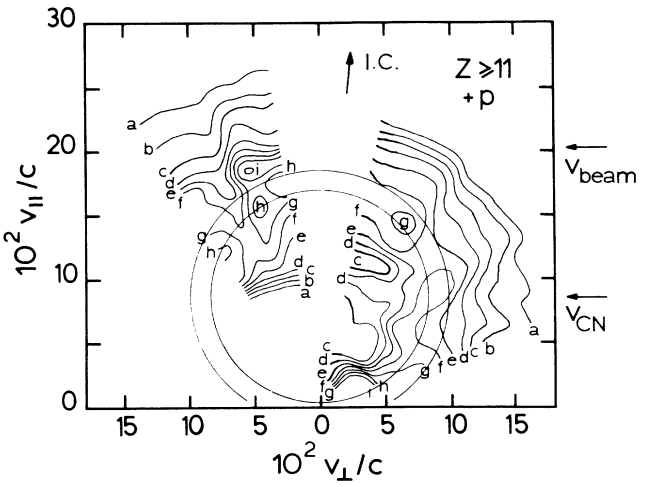

FIG. 5. Same as Fig. 3 except for protons. The contours correspond to 2, 4, 6, 8, 10, 12, 14, 16, and 18×10^4 mb $sr^{-1} c^{-3}$.

IV. FORMALISM

A. General

In order to understand the coincidence data we are faced with two choices: (1) to use an existing statistical model calculation to estimate the evaporation component, to subtract this, and to look at the remainder; or (2) to fit the data to some analytic approximation. In the present case the fused system must rid itself of nearly 220 MeV excitation energy. Calculations with the statistical-model code PACE,[15] modified to generate Monte Carlo coincidence events, cannot reproduce the light-particle energy spectrum shape even at backward angles. The data always extend to higher energies. Therefore, we have opted for the second alternative. This involves deriving a suitable parametrization of the coincidence data.

The coincidence between light particles and heavy residues introduces a kinematic bias into the observed spectra. In order to understand the underlying physics we must effectively remove this bias. For the rather complicated process of evaporation from a highly excited nucleus, most researchers attempt to simulate the observed data by way of a Monte Carlo computer calculation. This method has the advantage that it properly deals with the constraints of detector geometry. However, in practice the method is rather slow for coincidences (e.g., a single detector with an opening angle of a few degrees has roughly a 1% chance of seeing an event generated by the simulation, whereas a detector pair has $\sim 0.01\%$ chance of seeing a coincidence). In this way tens of thousands of computer events have to be generated, most of which are immediately thrown away. Moreover, one must run such a calculation many times under various assumptions in order to obtain the best agreement with the measured data.

In the limit of small detector solid angles (i.e., small enough such that the average of the cross section over the surface is equal, within the accuracy of the experiment, to the central value), one should be able to develop an analytic form that contains the coincidence kinematics, but that also has a number of free parameters. Such a function will provide a fast and reliable way of separating the physics from the kinematics. We have assumed that the light particle yield in fusion-like reactions comes from evaporation and from the emission of fast preequilibrium particles. Sections IV B and IV C give an analytic parametrization of these components.

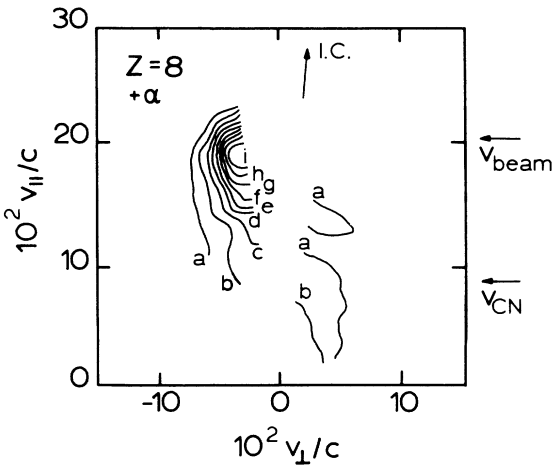

FIG. 4. The invariant velocity contours for α particles in coincidence with heavy residues at 5° with $Z = 8$. The contours, labeled *a* through *i*, begin with 10% of maximum cross section and increase in steps of 10%.

B. The evaporation component

Figure 6(a) shows the vector diagram for a simple description of evaporated particles in coincidence with

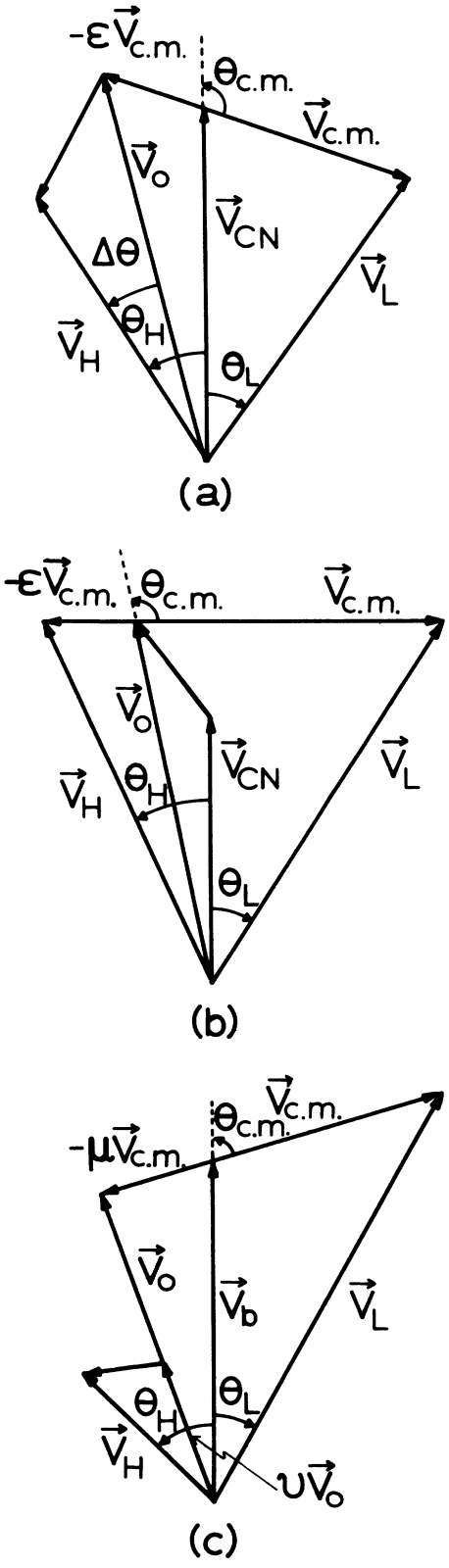

FIG. 6. Diagrams of the coincidence kinematics. (a) detected light particle is the first to be emitted; (b) detected light particle is the last to be emitted; and (c) a fast particle is emitted and the remainder of the projectile fuses with the target.

heavy residues. We begin with the assumption that, in the center-of-mass system, light particles are emitted governed by a transmission coefficient that reflects the Coulomb barrier E_c for particle emission

$$t(E_{\text{c.m.}})=\frac{1}{1+e^{-(E_{\text{c.m.}}-E_c)/T_c}}\ , \tag{6}$$

and an exponential term that specifies the number of available levels at a given excitation energy. If we assume that locally (in a given region of excitation energy) the change in the level density with energy is exponential, then the emitted light-particle spectra will have the form

$$\frac{d^2\sigma}{dE_{\text{c.m.}}d\Omega_{\text{c.m.}}}=\text{const}\times e^{-E_{\text{c.m.}}/T}t(E_{\text{c.m.}})P(\theta_{\text{c.m.}})\ , \tag{7}$$

where $P(\theta_{\text{c.m.}})$ is a possible angular dependence, T is a slope parameter related to the nuclear temperature, T_c is the dispersion of $t(E_{\text{c.m.}})$, and $(E_{\text{c.m.}},\theta_{\text{c.m.}})$ are the energy and angle of the emitted particle in the center of mass of the compound system. [Normally Eq. (7) would refer to the total kinetic energy E_{tot} in the center-of-mass frame. But since $E_{\text{tot}}=(1+\epsilon)E_{\text{c.m.}}$ (see definition of ϵ in the text), we can use Eq. (7) for $E_{\text{c.m.}}$, knowing that T, E_c, and T_c are $(1+\epsilon)$ times larger than the corresponding parameters with E_{tot}.] For the angular correlation function $P(\theta_{\text{c.m.}})$ we used the parametrization

$$P(\theta_{\text{c.m.}})=\frac{1}{\sqrt{\sin^2\theta_{\text{c.m.}}+k\cos^2\theta_{\text{c.m.}}}}\ . \tag{8}$$

Thus, for $k=0$ the classical $1/\sin\theta_{\text{c.m.}}$ limit is obtained, and as k goes from 0 to 1 the angular dependence becomes increasingly more isotropic.

The final distribution of HR's in velocity space results from a large number of small recoils that the HR receives during evaporation of particles. The central limit theorem of statistics insures that these velocities will be normally distributed provided that the number of evaporated particles is large ($\Delta A=20.5$ in our case) and that their emission is isotropic.[14] Experimental data bear out this assumption.[1]

Using Fig. 6(a) as our guide, let us assume that a nucleus moving with velocity $\mathbf{v}_{CN}$ emits a particle with velocity $\mathbf{v}_{\text{c.m.}}$ in its center-of-mass frame. The nucleus recoils with a velocity $-\epsilon\mathbf{v}_{\text{c.m.}}$, where ϵ is the ratio of masses for the emitted particle and recoiling nucleus. The heavy ions, due to subsequent evaporations, are normally distributed about $\mathbf{v}_0$:

$$\frac{d^2\sigma}{v_H^2 dv_H d\Omega_H}=\text{const}\times e^{-(\mathbf{v}_H-\mathbf{v}_0)^2/2\sigma^2}\ . \tag{9}$$

The coincidence cross section, then, is simply the product of Eqs. (7) and (9), with the kinematic constraint that relates $E_{\text{c.m.}}=\frac{1}{2}mv_{\text{c.m.}}^2$ and $\theta_{\text{c.m.}}$ to $\mathbf{v}_0$ [see Fig. 6(a)]. This can be transformed into the lab frame to yield:

$$\frac{d^4\sigma}{dE_L d\Omega_L dv_H d\Omega_H}=N\left[\frac{E_L}{E_{\text{c.m.}}}\right]^{1/2}\frac{e^{-E_{\text{c.m.}}/T}}{1+e^{-(E_{\text{c.m.}}-E_c)/T_c}}\times P(\theta_{\text{c.m.}})v_H^2 e^{-(\mathbf{v}_H-\mathbf{v}_0)^2/2\sigma^2} \tag{10}$$

with

$$\mathbf{v}_0=(1+\epsilon)\mathbf{v}_{CN}-\epsilon\mathbf{v}_L ,$$

$$E_{\text{c.m.}}=\tfrac{1}{2}mv_{\text{c.m.}}^2 ,$$

$$v_L\sin\theta_L=v_{\text{c.m.}}\sin\theta_{\text{c.m.}}$$

and

$$v_{\text{c.m.}}^2=v_{CN}^2+v_L^2-2v_Lv_{CN}\cos\theta_L .$$

The assumptions that have gone into this equation are the following: (1) The distribution of $\mathbf{v}_{CN}$ can be replaced by its average value; (2) ϵ is a constant; (3) the variation of σ in Eq. (9) as a function of HR mass can be ignored if replaced by some average value; and most importantly, (4) the detected particle is the first to come out of the system.

Normally, we are interested in using the HR detector as a trigger detector, and therefore Eq. (10) is only useful when integrated over the HR velocity. This yields

$$\frac{d^3\sigma}{dE_Ld\Omega_Ld\Omega_H}=N\left[\frac{E_L}{E_{\text{c.m.}}}\right]^{1/2}\frac{e^{-E_{\text{c.m.}}/T}}{1+e^{-(E_{\text{c.m.}}-E_c)/T_c}}\frac{1}{\left[k+(1-k)\dfrac{E_L}{E_{\text{c.m.}}}\sin^2\theta_L\right]^{1/2}}e^{-v_0^2/2\sigma^2}$$

$$\times\left[(\sigma^3+\sigma p^2)\Phi\left[\frac{p}{\sigma}\right]e^{p^2/2\sigma^2}+p\sigma^2\right] \tag{11}$$

with

$$p=v_0\cos\Delta\theta$$

$$=\cos\theta_H[(1+\epsilon)v_{CN}-\epsilon v_L\cos\theta_L]$$

$$-\epsilon v_L\sin\theta_L\sin\theta_H\cos(\phi_L-\phi_H) , \tag{12}$$

$$v_0^2=(1+\epsilon)^2v_{CN}^2+\epsilon^2v_L^2-2\epsilon(1+\epsilon)v_{CN}v_L\cos\theta_L , \tag{13}$$

and

$$\Phi(x)=\frac{\sqrt{\pi}}{2}\left[1+\text{erf}\left[\frac{x}{\sqrt{2}}\right]\right] .$$

We can integrate Eq. (10) over all variables and obtain

$$\sigma_{\text{tot}}^{\text{evap}}=N(2\pi)^{3/2}\sigma^3\pi\,\text{cosec}\left[\frac{\pi T_c}{T}\right]\frac{4\pi}{\sqrt{1-k}}$$

$$\times\arcsin(\sqrt{1-k})T_ce^{-E_c/T} , \tag{14}$$

assuming that Eq. (7) is zero for $E_{\text{c.m.}}<0$ (this is valid when $E_c\gg T_c$). Unfortunately, we were unable to derive an analytic form for the cross section $d\sigma/d\Omega_H$ which would allow us to calculate light-particle multiplicities with a simple formula. In this case we have resorted to numerical integration.

Equations (10)–(14) rely on the assumption that the light particle is the first to come out of the reaction; this is, of course, true for only one of many evaporated particles. To check the influence of this assumption on the deduced formulas, we assumed the opposite situation [see Fig. 6(b)] in which the HR's first achieve some distribution through evaporations. Then, in the final stage of the reaction, a particle emerges which is detected. The cross section now takes a slightly different form:

$$\frac{d^4\sigma}{dv_Hd E_Ld\Omega_Hd\Omega_L}=\frac{N}{(1+\epsilon)^3}\left[\frac{E_L}{E_{\text{c.m.}}}\right]^{1/2}\frac{e^{-E_{\text{c.m.}}/T}}{1+e^{-(E_{\text{c.m.}}-E_c)/T_c}}$$

$$\times P(\theta_{\text{c.m.}})v_H^2e^{-(\mathbf{v}_H-\epsilon\mathbf{v}_{\text{c.m.}}-\mathbf{v}_{CN})^2/2\sigma^2} \tag{15}$$

with

$$\mathbf{v}_{\text{c.m.}}=\frac{\mathbf{v}_L-\mathbf{v}_H}{1+\epsilon} ,$$

$$E_{\text{c.m.}}=\tfrac{1}{2}mv_{\text{c.m.}}^2 , \tag{16}$$

$$\mathbf{v}_L\cdot\mathbf{v}_H=v_Hv_L[\sin\theta_L\sin\theta_H\cos(\phi_H-\phi_L)+\cos\theta_L\cos\theta_H] ,$$

and

$$\cos^2\theta_{\text{c.m.}}=\frac{[\mathbf{v}_H\cdot\mathbf{v}_L(1-\epsilon)+\epsilon v_L^2-v_H^2]^2}{v_0^2v_{\text{c.m.}}^2(1+\epsilon)^4} . \tag{17}$$

Although the integral of Eq. (15) over all variables yields Eq. (14), we were unable to derive the analytical equivalent of Eq. (11). Therefore, this limit requires a numerical integration. Section IV D compares the two forms, Eq. (10) and Eq. (15).

C. The preequilibrium component

Whether the preequilibrium emission of particles come from Fermi jets[3] or fragmentation,[16,17] one can accurately express the light-particle velocity distributions in the center-of-mass of their source as a Gaussian with separate widths for the directions parallel ($\sigma_\parallel$) and perpendicular ($\sigma_\perp$) to the beam. These widths are generally determined by the intrinsic momentum of the escaping particles, modified by various nuclear dynamical effects. Whatever the mechanism may be, however, such a Gaussian may reasonably describe it. The preequilibrium cross section is

$$\frac{d^3\sigma}{d^3v_{\text{c.m.}}}=\text{const}\times e^{-(v_\parallel^2/2\sigma_\parallel^2+v_\perp^2/2\sigma_\perp^2)} \tag{18}$$

in the center-of-mass frame of this fast source. In the context of nuclear fragmentation $\sigma_\perp$ and $\sigma_\parallel$ are related to the size of the fragment which travels (on average) at nearly the beam velocity:

$$m^2\sigma_\parallel^2=[K(A_p-K)/(A_p-1)]\sigma_0^2 ,$$

$$m^2\sigma_\perp^2=m^2\sigma_\parallel^2+\frac{K(K-1)}{A_p(A_p-1)}\sigma_1^2 , \tag{19}$$

with $\sigma_0 \approx 90$ MeV/c,[17] $\sigma_1 \approx 200$ MeV/c for reactions at ≈ 100 MeV/nucleon,[18] K is the fragment mass number, A_p is the mass number of the projectile that breaks up in the field of the target number, and m is the fragment mass.

We can use the geometry of Fig. 6(c) to calculate the coincidence fragmentation cross section. It is

$$\frac{d^4\sigma}{dv_L d\Omega_L dv_H d\Omega_H} = N_f v_L^2 v_H^2 e^{-(\mathbf{v}_L-\mathbf{v}_b)_\perp^2/2\sigma_\perp^2} e^{-(\mathbf{v}_L-\mathbf{v}_b)_\parallel^2/2\sigma_\parallel^2} \times e^{-(\mathbf{v}_H-v(1+\mu)\mathbf{v}_b+\mu v\mathbf{v}_L)^2/2\sigma^2} \quad (20)$$

with

$$\mu = \frac{K}{A_p - K}$$

and

$$v = \frac{A_p - K}{A_t + A_p - K} .$$

A_t is the target mass number. Integrated over the heavy-ion velocity and converted to energy variables, this becomes

$$\frac{d^3\sigma}{dE_L d\Omega_L d\Omega_H} = N_F \left[\frac{2E_L}{m^3}\right]^{1/2} e^{-(\sqrt{E_L}\cos\theta_L - \sqrt{E_b})^2/m\sigma_\parallel^2} e^{-E_L\sin^2\theta_L/m\sigma_\perp^2} e^{-v^2 v_0^2/2\sigma^2} \left[(\sigma^3+\sigma p^2)\Phi\left[\frac{p}{\sigma}\right] e^{p^2/2\sigma^2} + p\sigma^2\right] \quad (21)$$

with

$$\mathbf{v}_0 = (1+\mu)\mathbf{v}_b - \mu\mathbf{v}_L , \quad E_L = \tfrac{1}{2}mv_L^2 , \quad E_b = \tfrac{1}{2}mv_b^2 ,$$

and

$$p = \cos\theta_H[v(1+\mu)v_b - \mu v v_L\cos\theta_L] - \mu v v_L \sin\theta_H \sin\theta_L \cos(\phi_H - \phi_L) .$$

Integration of Eq. (20) over all light-particle variables gives the singles evaporation residue cross section:

$$\frac{d^2\sigma}{v_H^2 dv_H d\Omega_H} = N_f (2\pi)^{3/2} \frac{\sigma_\perp^2 \sigma_\parallel \sigma^3}{u_\perp^2 u_\parallel} e^{-v_H^2\sin^2\theta_H/2u_\perp^2} \times e^{-(v_H\cos\theta_H - vv_b)^2/2u_\parallel^2} \quad (22)$$

in which $u_\perp^2 = \sigma^2 + \mu^2 v^2 \sigma_\perp^2$ and $u_\parallel^2 = \sigma^2 + \mu^2 v^2 \sigma_\parallel^2$. Equation (22), when summed over heavy-ion velocities, yields:

$$\frac{d\sigma}{d\Omega_H} = N_f (2\pi)^{3/2} \sigma_\perp^2 \sigma_\parallel \sigma^3 \left[\frac{u_\perp u_\parallel^2}{g^3}\right] \times [(1+x^2)\Phi(x) + xe^{-x^2/2}] e^{-y^2/2} \quad (23)$$

with

$$g^2 = \mu^2 v^2 \cos^2\theta_H \sigma_\perp^2 + \mu^2 v^2 \sin^2\theta_H \sigma_\parallel^2 + \sigma^2 ,$$

$$x = v v_b \left[\frac{u_\perp}{g u_\parallel}\right] \cos\theta_H , \quad (24)$$

and

$$y = \frac{v v_b}{g} \sin\theta_H .$$

A final integration over all variables produces:

$$\sigma_{\text{tot}}^{\text{fast}} = (2\pi)^3 N_f \sigma^3 \sigma_\perp^2 \sigma_\parallel . \quad (25)$$

D. Model dependence of the parameters

In the following paragraphs we would like to address the problem of model dependence of the extracted parameters as well as the uniqueness of the fitted solution. As reference functions we have chosen Eq. (11) for the description of the evaporation spectra, and Eq. (21) with $\sigma_\parallel = \sigma_\perp$ for the fast component. The α spectra provided the best quality data for our comparisons. Column a of Table II lists the best-fit parameters under these assumptions. In this case, as well as in all subsequent analysis, we have simultaneously fit all 14 angles in the angular distribution to one set of parameters using a simplex fitting routine.[19] Since the width σ of the heavy-ion distribution should not differ much for the fast and evaporation components, we have used a single value for both.

If, however, the added kick given to the heavy ion due to the detected particle is significantly different in the cases of fast emission and evaporations, σ may differ slightly. Column b in Table II lists the best-fitting parameters given two separate widths. The overall fit is not improved even though the data seem to favor a σ that is 10% smaller in the evaporation case than for the fast component. The slight difference also does not affect the extracted multiplicities to a large degree. Hence, we feel that it is unnecessary to use a separate σ for the two components.

Perhaps a more important question concerns the effect of multiplying Eq. (7) by a factor $\sqrt{E_{\text{c.m.}}}$. This choice may in fact more closely reflect the level densities in the nucleus, and has the advantage of eliminating the singularity at $E_{\text{c.m.}} = 0$ in Eq. (10). Column c of Table II shows that this form does not improve the fit, nor affect the extracted multiplicities significantly. An important point, however, is that the extracted value for T is 20% smaller in this case. Tests with angle-integrated center-of-mass α energy spectra generated for ^{20}Ne + ^{27}Al using

TABLE II. Fit parameters produced with various assumptions about the model functions.

	a	b	c	d	e	f
V_{CN}/c	0.0799	0.0799	0.0765	0.0789	0.0841	
ϵ	0.164	0.166	0.231	0.095	0.127	
k	0.194	0.627	0.199	0.528	0.244	0.25
T (MeV)	15.9	16.4	13.0	12.2	17.7	10.9
σ/c	0.0142	0.0136	0.0163	0.0105	0.0186	
T_c (MeV)	1.91	1.94	2.37	1.78	2.48	1.4
E_c (MeV)	6.80	6.62	6.86	6.66	7.58	6.0
M_{evap}	3.42	3.24	3.92	2.83		2.6
v_b/c	0.192	0.187	0.187	0.189		
μ	0.218	0.215	0.198	0.166		
v	0.688	0.651	0.703	0.450		
$\sigma_\parallel/c$	0.0349	0.0344	0.0392	0.0315		
M_{fast}	0.22	0.32	0.27	0.33		
σ'/c		0.0152				
$\sigma_\perp/c$				0.0379		
χ^2	2.10	2.10	2.30	1.87		

[a]Reference fit.
[b]Fit with separate widths for fast (σ') and evaporation (σ) components.
[c]Fit with evaporative component multiplied by $\sqrt{E_{\text{c.m.}}}$.
[d]Fit with both parallel and perpendicular widths for the fast component.
[e]Fit with Eq. (11) to "data" generated from the last-out equations [Eq. (15)] using the parameters of column a.
[f]PACE results for $l_{cr}=47\hbar$.

the code PACE also show that adding a factor of $\sqrt{E_{\text{c.m.}}}$ reduces the extracted T by $\approx 25\%$ and E_c by $\approx 10\%$.

Until now we have held the widths $\sigma_\perp$ and $\sigma_\parallel$ equal to each other. Freeing the fit from this constraint produces column d of Table II. The fit in this case is significantly better. Even in the case where $\sigma_\parallel$ is chosen twice as large as $\sigma_\perp$ at the start of the fit, the data prefer a slightly larger $\sigma_\perp$. This is consistent with the trends observed in the fragmentation studies of Van Bibber *et al.*[18] The added width in $\sigma_\perp$ spreads the fast component out to larger angles, thus allowing T to be a bit smaller.

In all of the above fits we have assumed that the detected evaporation particle is the first to come out of the system. How much does this assumption bias our results? Given that Eq. (10) is one limit (first-out) then Eq. (15) should be the opposite limit (last-out). If we can show that the two equations, integrated over heavy-ion velocity, can both describe the same coincidence data, albeit with different sets of parameters, then we can set limits on these parameters within our model. Since Eq. (15) has to be integrated numerically, it was far too slow for normal use in the simplex fitting program. However, we can convince ourselves that the two functions can produce equivalent curves at all angles. Let us suppose the last-out function is used to generate spectra for all in-plane angles less than 90° in the lab system at 10° intervals. Then, the first-out function can easily be used to fit these data. Column e in Table II shows the results of such a fit for a last-out data set generated with the parameters of column a. Figure 7 shows the first-out (solid lines) and last-out (dashed lines) functions for various lab angles. Although there are slight variations between the two functions, these are small, and generally confined to energies below the Coulomb barrier. Therefore, we are confident that any estimate of the evaporation using the first-out function will not misrepresent that component. The interpretation of the extracted parameters, however, does depend on the particular function used. By comparing columns a and e one can readily see the variations in parameters between first-out and last-out functions. Assuming that the average values of the parameters for the two cases best reflect the physics, then for fits with the

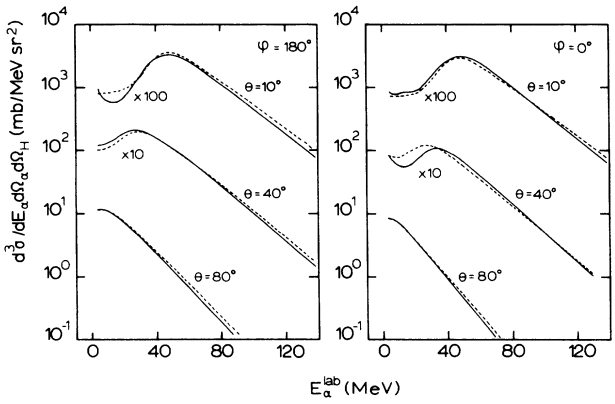

FIG. 7. Comparisons between first-out (solid lines) and last-out (dashed lines) functions. See text and Table III for parameters.

first-out function: v_{CN} is too large by $\approx 3\%$, ϵ is too small by $\approx 15\%$, k is too large by $\approx 10\%$, T is too large by $\approx 5\%$; σ is too large by $\approx 12\%$; T_c is too large by $\approx 11\%$, and E_c is too large by $\approx 5\%$. All of these shifts agree with intuition: first smearing out the HR distribution and then emitting a particle will produce a spectrum which appears to have a more relaxed fall-off with energy, a less sharply forward-peaked angular distribution, and a more relaxed cutoff below the Coulomb barrier.

Column f lists the corresponding parameters deduced using the statistical model code PACE (Ref. 15) for the completely fused $^{20}Ne + {}^{27}Al$ system at 19.2 MeV/nucleon incident energy. The code makes use of rotating liquid drop model level densities at high excitation energy and a triangular angular momentum distribution with $l_{cr} = 47\hbar$, deduced from evaporation residue cross sections.[13] The value T is rather insensitive to reasonable variations in l_{cr} and is smaller than the experimental values. The average Coulomb energy E_c, however, is in reasonable agreement with the values extracted from the coincidence data.

Since the extracted value T is larger than one might expect from the statistical model, and M_{fast} is remarkably small, we have asked ourselves the question whether the fit has unfairly divided the data into two pieces. If v_b were smaller, for example, then more of the preequilibrium component could extend to larger angles. In order to test this, we have performed a series of fits with v_b fixed ranging from $0.14c$ to $0.22c$, again using the standard fit function described above.

First two trivial cases were considered: (1) only evaporation and (2) only fast particles. Neither component alone can describe the data. The fit to only evaporation left considerable cross section at forward angles unaccounted for. On the other hand, the fit to fast particles alone could not reproduce the low-energy end of the spectra at forward angles, and fell off too rapidly to account for the backward angles.

For each value v_b from $0.14c$ to $0.22c$ in steps of $0.01c$ we allowed all other parameters to vary freely. For the points in the middle of this range two or three separate sets of starting values were chosen to let the fit procedure converge to a false minimum. The best χ^2 values (always normalized by the number of degrees of freedom) ranged from 1.9 to 2.9 with a minimum for $v_b = 0.185c$. Over the full range, $\sigma_{\parallel}$ fell linearly ($0.05c - 0.02c$) with v_b, and M_{fast} fell almost exponentially (0.9 to 0.1) with v_b. The smallest values of T and M_{evap}, however, occurred for $v_b \approx 0.185c$.

Morgenstern *et al.*[1] have measured a momentum shift for the singles ER spectra of $\approx 15\%$. We can estimate the contribution to this momentum shift that our fast α particles produce. However, since this shift is roughly proportional to $v_b M_{\text{fast}}$, the lower velocities tend to cancel the larger multiplicities. Over the range $v_b = 0.14c$ to $0.22c$ the deduced momentum shift varies from $\approx 6\%$ down to $\approx 1\%$ with the value $\approx 3\%$ at $v_b = 0.185c$. No matter how the α spectra are divided into two components, not more than about $\frac{1}{3}$ of the momentum deficit observed in inclusive measurements can be accounted for.

V. RESULTS

A. The fitted LP spectra

In the previous sections only the alpha spectra have been discussed. Although the p, d, t, and ^3He spectra are not of as high quality, we still can obtain useful information from them as well. The proton spectra suffer from the fact that only the CsI detector could stop protons with energies above 30 MeV. Hence, any extractions of fast protons from the data will be rather inaccurate. The other light-particle spectra, on the other hand, contain rather large statistical error bars, and one simply does not have the information to deduce all of the parameters in the model from these data. However, with reasonable assumptions, the multiplicities of each LP can be estimated.

Given these limitations, we have fixed the parameters v_{CN}, T, σ, T_c, and E_c to the values deduced from the α spectra, set k to 1, scaled ϵ, μ, and v to account for differences in emitted particles masses, and taken $\sigma_{\parallel}$ and $\sigma_{\perp}$ from the alpha results using Eq. (19). This equation is valid for fragmentation and may not properly describe the proton data. First all values except the magnitudes of each component were fixed. Then the restrictions on the other parameters were gradually loosened until the χ^2 had fallen to within reasonable limits. Table III lists the final results for each light particle.

Table IV lists the multiplicities deduced from our data. A sum of the multiplicities, weighted by the number of nucleons in each LP, should add up to the average number of nucleons emitted from $Z \geq 11$ residues. From singles experiments[13] we know this number to be 20.5. The data of Table IV yield 18.4 in reasonable agreement with expectations. This also lends support to our observation that heavier fragments such as Li and Be contribute very little to the fusion-like spectra. This does not necessarily mean that evaporation of heavy fragments is not important, but merely that if such fragments are emitted, they quite probably decay into LP's with $Z \leq 2$. Figure 8 shows the coincidence α particle spectra together with the decomposition into two components. Plotted are the differential α particle multiplicities (i.e., cross sections normalized to the singles $Z \geq 11$ HR cross section at $\theta_H = 5°$) as a function of the laboratory α particle energy. The sum of the fast and evaporative contributions nicely passes through the data at all angles. The fast component (dots) is little more than a small, extremely broad contribution that shows up at small angles.

Figure 9 shows the cross section contours in velocity space deduced from the fits to the α spectra. The contours, in steps of 10% of the maximum cross section, generally increase from the boundaries towards the center of each plot. The evaporation of α particles (c) displays a peaking in forward as well as in backward (in this case near zero velocity in the lab) directions and a marked hole half way between due to the Coulomb barrier. This graph shows exactly the same features as Fig. 3, the peak slightly to the left of the beam direction, the minimum near the compound nuclear velocity, and an increase in the cross section at low lab velocities. This seemingly

TABLE III. Final fit parameters for coincident LP spectra. Errors for proton and α spectra are quoted in parentheses in %.

	p	d	t	^{3}He	α
v_{CN}/c	0.102(2)	0.078	0.078	0.078	0.0780(1)
ϵ	0.866(96)	0.0743	0.111	0.111	0.148(6)
k	1(13)	1	1	1	0.614(11)
T (MeV)	9.31(6)	13.2	16.6	16.4	16.6(4)
σ/c	0.104(20)	0.0124	0.0124	0.0124	0.0124(10)
T_c (MeV)	0.794(3)	1.06	1.67	1.77	1.77(2)
E_c (MeV)	3.52(4)	3.94	5.25	8.02	6.52(2)
M_{evap}	1.26(9)	0.50	0.14	0.11	3.32(11)
v_b/c	0.145(2)	0.189	0.189	0.189	0.189(2)
μ	0.0415(468)	0.111	0.176	0.176	0.177(12)
v	0.433(23)	0.400	0.386	0.386	0.545(9)
$\sigma_\parallel/c$	0.0509(6)	0.0311	0.0367	0.0540	0.0308(3)
M_{fast}	0.60(24)	0.042	0.014	0.046	0.30(14)
$\sigma_\perp/c$	0.0810(4)	0.0633	0.0391	0.0648	0.0340(2)
χ^2	3.92	1.57	1.49	1.39	1.81

complicated shape arises from the coincidence kinematics and the light-particle anisotropy built into the formalism. If the α particles were emitted isotropically (d) one would still see a focusing of the cross section at backward angles stemming from the fact that the ionization chamber selectively enhances decays that send LP's in the opposite direction from the detected HR. The fast component (b) has a simple shape, but it too peaks slightly to the left of the beam axis. The sum of fast and evaporative components (a) bears most of the features of evaporation since the preequilibrium contribution is relatively small. Although Figs. 9(a) and 3 contain all of the same features, they look somewhat different at first glance and cannot be used for precise comparisons between data and fits. The undulation in the contour lines of Fig. 3 is an artifact produced by the averaging routine that fills in the gaps between detectors. Likewise, this routine also distorts the contours at small velocities in the lab system near detector thresholds.

Figure 10 gives the proton data with the respective decomposition. For the present reaction the beam velocity is (accidentally) nearly equal to the sum of the compound nuclear velocity plus the Coulomb velocity for proton emission. Therefore, both components peak at almost the same proton lab energy. Fortunately, the two contributions have differing angular distributions and, hence, a separation is possible.

B. Discussion

Since each parameter is very strongly correlated with many of the others, it is unreasonable to merely quote the statistical errors associated with the fits. For each LP we have performed at least 10 different fits with different starting values. Each of the final fits having a χ^2 value within 10% of the minimum χ^2 and a visually reasonable description of the data, determined the variations in the parameters. The quoted errors in Tables III and IV are therefore the larger of either the statistical errors from the fits, or the rms variations from fit to fit. The difference between Table II, column d and the results for α particles in Table III shows the effect of choosing slightly different initial parameters.

Systematic errors due to solid angle determinations are in the neighborhood of 10%. Perhaps the largest systematic error introduced into the multiplicity determinations comes from the assumption that on the basis of in-plane measurements one can deduce the out-of-plane contributions. If the θ anisotropy deduced from the in-plane data is not severe ($k \approx 1$) then any ϕ dependence should be negligible. For all LP's other than α particles, $k = 1$ is consistent with the data. For α particles, the value $k \approx 0.6$ is large enough to keep us from worrying about the ϕ dependence. However, the value M_{evap} for α's may be slightly too large.

TABLE IV. Light-particle multiplicities for fusion-like events.

	M_{clust}	M_{fast}	M_{evap}	M_{tot}	M_{PACE}
p	0.17	0.45±0.11	1.37±0.13	1.82±0.17	5.3
d	0.21	0.043±0.007	0.49±0.04	0.54±0.04	
t	0.17	0.016±0.003	0.12±0.02	0.13±0.02	
^{3}He	0.11	0.034±0.013	0.15±0.05	0.18±0.04	
α	4.71	0.36±0.05	2.84±0.30	3.19±0.26	2.6
n	0.20	(0.45±0.011)	(1.37±0.13)	(1.82±0.17)	5.0
Total	20.5	2.6±0.3	15.9±1.2	18.4±1.1	20.7

From singles systematics[1] the equivalent of roughly five preequilibrium beam-velocity nucleons is expected. The total in Table IV is only half that value. Equation (4) indicates that neutron emission is not significantly favored over proton emission. Hence, the fast neutron multiplicities must be similar to the proton multiplicities. On the other hand, the combined effect of $Z>2$ fragments, though of very low multiplicity, could make up the difference. The LP multiplicities for the evaporation component are somewhat more accurate, and since these are the major contribution to the total multiplicity, we can account for nearly all of the emission from fusion-like events. This is consistent with our observations that the multiplicities of particles heavier than α particles were small.

The fast component in the α spectrum agrees with the systematics of fragmentation fusion as calculated in the framework of a direct-transfer model[20] as well as with data taken at 20 MeV/nucleon for $^{20}\mathrm{Ne}+{}^{197}\mathrm{Au}$.[21] These results are $m\sigma_{\parallel}=74$ and 76 ± 4 MeV/c, respectively. Our value of 63 ± 2 MeV/c, though a bit smaller, is reasonably close to these results. The fact that $m\sigma_{\perp}$ is larger than $m\sigma_{\parallel}$ agrees with Eq. (19). Our data yield $\sigma_1=300\pm6$ MeV/c in comparison with 200 MeV/c for fragmentation at 100 MeV/nucleon.[18] Since the added width comes from an interaction of the fragment with the rest of the system, one should expect that, at lower energies where one of the fragments fuses with the target, the perpendicular component will be considerably larger than at high energies. The relative yields of ^{3}He with respect to ^{4}He is about 0.1; this is also predicted by Christov and observed in the Ne + Au system.[20] These authors also see very few fragments heavier than α particles. Our results for α particles, therefore, are indeed consistent with a fragmentation-fusion picture of incomplete fusion.

The proton data are a bit more difficult to interpret. The parameters ϵ and σ in Table III are unexpectedly large, which suggests that the many-body kinematics for such light particles may not be properly described in our simple model. In addition, beam velocity protons tend to peak at nearly the same lab energies as protons evaporated into forward angles. Hence, without good high-energy data, we cannot accurately determine all of the model parameters. Limits can, however, be placed on the multiplicities. Fitting the data only to a fast component, yields a distribution peaking at $v_b=0.12c$ with $M_{\mathrm{fast}}=1.45$ and $\chi^2=11.3$. The opposite extreme, all evaporation, yields

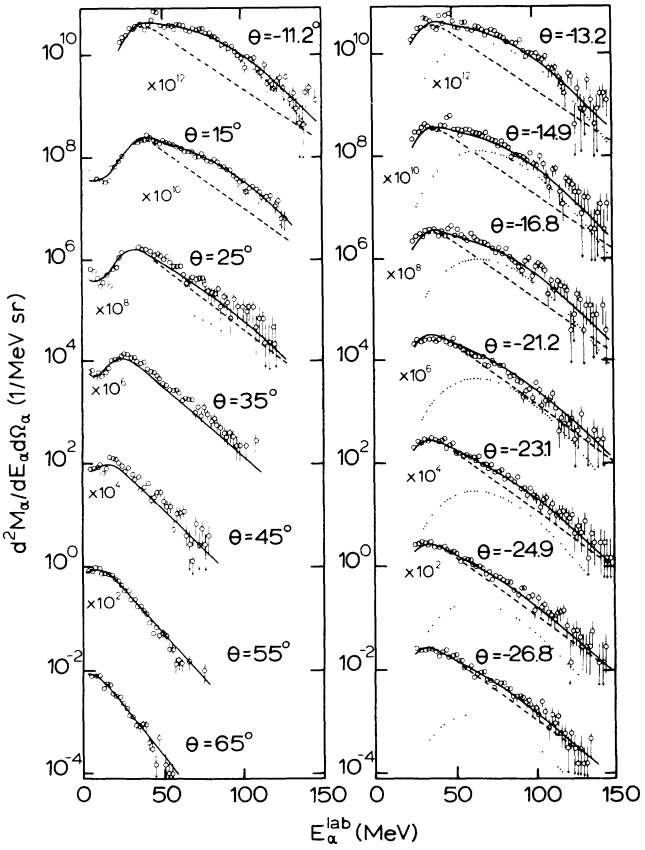

FIG. 8. Coincident alpha spectra with best-fitting parametrization.

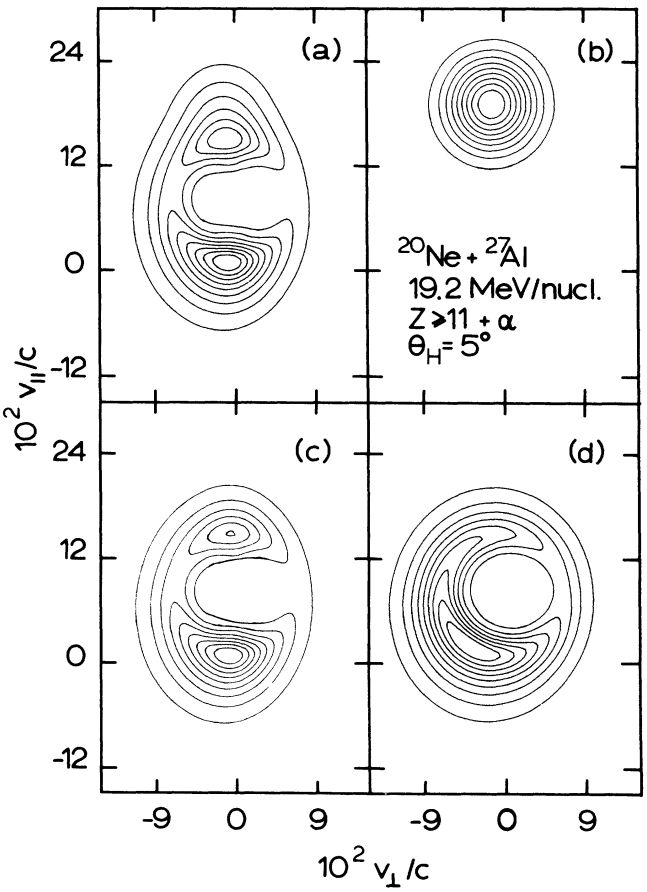

FIG. 9. Velocity-invariant contours for fitted functions for alpha particles. (a) Best fit to evaporation plus fast components; (b) fast component only; (c) evaporation component only; and (d) evaporation component with angular distribution coefficient k set to 1.

$T=7.0$ MeV, $M_{\text{evap}}=1.81$ and $\chi^2=6.1$. It is indeed surprising that the total proton multiplicity is not larger than 2, no matter how the spectrum gets divided. According to simple calculations of Fermi jets,[3] $\sigma_\perp=0.054c$, $\sigma_\parallel=0.047c$, and $v_b=0.17c$ in the Gaussian approximation can be expected for our system. Moreover, this model predicts 5.7 jetted nucleons from both partners in the Ne + Al system; these nucleons, however, account for only $\frac{1}{4}$ of the singles velocity shift. For light systems, one expects equal numbers of neutrons and protons to be emitted. From Table IV we conclude that our results are consistent with the prediction that $\frac{1}{4}$ of the velocity shift comes from nucleons, but we simply do not see the high proton multiplicities predicted by the model. Since the Fermi jet calculations include only mean-field effects, one possible explanation for this discrepancy could be that the jetting mechanism is already quite inhibited at 20 MeV/nucleon by nucleon-nucleon collisions.

Table IV lists multiplicities M_{clust} calculated from the inclusive mass and element distributions measured by Bakkum *et al.*[13] These values represent the extreme limit of maximal clustering, that is, that 2 protons and 2 neutrons will always form an alpha particle, one neutron and one proton a deuteron; etc. Clearly, this overestimates the α yield and underestimates the nucleon multiplicities.

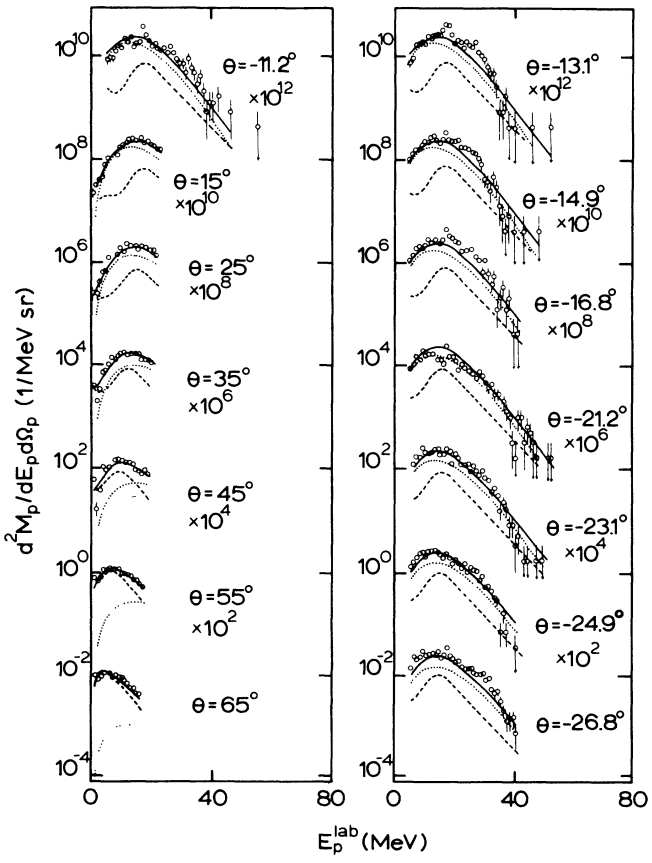

FIG. 10. Coincident proton spectra with best-fitting parametrization.

However, it does show a remarkable tendency of the ^{20}Ne + ^{27}Al system to prefer α emission over 4 nucleon emission.

The evaporation results offer a few surprises. The multiplicity for alpha particles is quite high compared to other light-particle emission. Also, despite the qualifications in the previous sections concerning T, the observed α particles favor larger energies than expected from the statistical model. The fact that the extracted temperature parameter T is larger for α particles than for protons agrees with the general observation in moving source parametrizations of singles LP data that the deduced temperatures increase systematically from protons to heavier $Z=1,2$ isotopes.[22] If v_{CN} is spread over a range of values (due to the ICF process), T will be too large. Since the ICF velocity shift is small, however, T will not be altered by more than about 10%. Moreover, this should affect protons and α's equally. The observed T values could be explained by the evaporation of hot fragments which sequentially decay. Since light nuclei decay predominantly by α emission, this would explain the difference in the T values for protons and heavier particles. If this process is important one should be able to see definite LP-LP correlations for fusion-like events. Experimentally, this would require a difficult triple coincidence experiment to effectively isolate the fusion-like processes.

There is theoretical evidence that collective effects can make light-particle spectra appear to be produced at larger than actual temperatures.[23] Additionally, recent Vlasov-Uehling-Uhlenbeck (VUU) calculations that include no reaction dynamics, but begin with an equilibrated system at high temperature [^{40}Ar at $T=15$ MeV (Ref. 24)], show a marked, nearly isotropic expansion from $r=5$ to 6.8 fm during a time scale of ~ 50 fm/c. Alpha particles should be emitted from the nuclear surface, hence, those emitted during such an expansion process would carry an additional velocity due to the collective motion. Protons, however, which are presumably emitted from the nuclear interior as well as from the surface, should not be as sensitive to this collective motion and should more closely indicate the actual temperature of the system. If such a scenario is true, then the difference between measured T values for proton's and α's could provide an experimental determination of the expansion velocity.

VI. CONCLUSIONS

For the case of ^{20}Ne + ^{27}Al at 20 MeV/nucleon, it is possible to separate the fusion-like events from other processes by measuring the charges and energies of evaporation residues. Measuring LP's in coincidence with these ER's produces a clean set of spectra containing information on the LP emission from fusion-like processes. Since the coincidence requirement alters the shape of the LP spectra, one needs to apply some correction for the kinematics. The coincidence moving-source parametrization developed in this paper provides a simple way of removing this kinematic bias. Two sources, an evaporative and a preequilibrium component, are necessary but also sufficient to describe the energy and angular distributions

of the fusion-like LP spectra. The data show a large amount of α clustering in the evaporation from a compound system. The extracted temperature parameter T for α particles is much larger than expected from the statistical model. This is an interesting effect that merits further study. LP's with $Z \leq 2$ account for roughly 90% of the mass lost from the $^{20}Ne + {}^{27}Al$ system during and after fusion. The data for α particles show no sharp peak at the beam velocity as expected in the simplest pictures of ICF. On the contrary, these fast α particles are distributed over a wide range of energies consistent with a fragmentation-fusion picture. These fragments, however, only account for $\frac{1}{3}$ of the momentum lost due to ICF at 20 MeV/nucleon. Some, but not all, of the remaining $\frac{2}{3}$ appears in the p, d, t, and ^{3}He channels.

The picture that has emerged from the present study is one that shows the richness of reactions at intermediate energy. The process of nuclear fragmentation observed at 100 MeV/nucleon appears to have its counterpart at 20 MeV/nucleon where the probability is high that one of the fragments is absorbed by the target. But fragmentation fusion does not account for all of the escaping momentum. Nucleon emission, from whatever cause, plays a role. In addition, the nature of LP evaporation from systems at high temperatures is more complicated and interesting than extrapolations from lower temperatures would imply. Understanding the precise behavior of these hot nuclei remains an interesting problem for the years to come.

ACKNOWLEDGMENTS

We would like to thank the staff of the Kernfysisch Versneller Instituut in Groningen for providing us with the ^{20}Ne beam. This work was part of the research program of the "Stichting Fundamenteel Onderzoek der Materie" (FOM) with financial support from the "Nederlandse Organisatie voor Zuiver-Wetenschappelijk Onderzoek" (ZWO).

---

*On leave from the Institute of Experimental Physics, University of Warsaw, Poland.

[1]H. Morgenstern, W. Bohne, K. Grabisch, H. Lehr, and W. Stoeffler, Z. Phys. A **313**, 39 (1983).

[2]C. Gregoire and F. Scheuter, Phys. Lett. **146B**, 21 (1984).

[3]K. Moehring, W. J. Swiatecki, and M. Zielinska-Pfabe, Nucl. Phys. **A440**, 89 (1985).

[4]J. P. Bondorf, J. N. De, G. Fai, A. O. T. Karvinen, B. Jakobsson, and J. Randrup, Nucl. Phys. **A333**, 285 (1980).

[5]M. Blann, Phys. Rev. C **31**, 1245 (1985).

[6]J. Wilczynski, K. Siwek-Wilczynska, J. van Driel, S. Gonggrijp, D. C. J. M. Hageman, R. V. F. Janssens, J. Lukasiak, R. H. Siemssen, and S. Y. van der Werf, Nucl. Phys. **A373**, 109 (1982).

[7]T. Udagawa and T. Tamura, Phys. Rev. Lett. **45**, 1311 (1980).

[8]H. Morgenstern, W. Bohne, W. Galster, and K. Grabisch, Z. Phys. A **324**, 443 (1986).

[9]R. H. Siemssen, G. J. Balster, H. W. Wilschut, P. D. Bond, P. C. N. Crouzen, P. B. Goldhoorn, Han Shukui, and Z. Sujkowski, Phys. Lett. **161B**, 261 (1985); and G. J. Balster, R. H. Siemssen, and H. W. Wilschut, Nucl. Phys. **A471**, 635 (1987).

[10]H. Ikezoe, N. Shikazono, Y. Tomita, Y. Sugiyama, and K. Ideno, Nucl. Phys. **A462**, 150 (1987).

[11]E. Holub, D. Hilscher, G. Ingold, U. Jahnke, H. Orf, and H. Rossner, Phys. Rev. C **28**, 252 (1983).

[12]R. J. Meijer, A. van den Brink, E. A. Bakkum, P. Decowski, K. A. Griffioen, and R. Kamermans, Nucl. Instrum. Methods A **256**, 521 (1987).

[13]E. A. Bakkum, thesis, University of Utrecht, The Netherlands, 1988.

[14]J. Gomez del Campo, R. G. Stokstad, J. A. Biggerstaff, R. A. Dayras, A. H. Snell, and P. H. Stelson, Phys. Rev. C **19**, 2170 (1979).

[15]A. Gavron, Phys. Rev. C **21**, 230 (1980).

[16]A. S. Goldhaber, Phys. Lett. **53B**, 306 (1974).

[17]M. J. Murphy, Phys. Lett. **135B**, 25 (1984).

[18]K. Van Bibber, D. L. Hendrie, D. K. Scott, H. H. Weiman, L. S. Schroeder, J. V. Geaga, S. A. Cessin, R. Treuhaft, Y. J. Grossiord, J. O. Rasmussen, and C. Y. Wong, Phys. Rev. Lett. **43**, 840 (1979).

[19]M. S. Caceci and W. P. Cacheris, Byte Magazine, May 1984, 340.

[20]Chr. V. Christov, Z. Phys. A **325**, 221 (1986).

[21]Ch. Egelhaaf, M. Bürgel, H. Fuchs, A. Gamp, H. Homeyer, D. Kovar, and W. Rauch, Nucl. Phys. **A405**, 397 (1983); H. Homeyer, M. Bürgel, Ch. Egelhaaf, H. Fuchs, and G. Thoma, Z. Phys. A **319**, 143 (1984).

[22]C. B. Chitwood, D. J. Fields, C. K. Gelbke, D. R. Klesch, W. G. Lynch, M. B. Tsang, T. C. Awes, R. L. Ferguson, F. E. Obenshain, F. Plasil, R. L. Robinson, and G. R. Young, Phys. Rev. C **34**, 858 (1986).

[23]P. Mädler, L. Münchow, and A. Pfitzner, *Proceedings of the XVIth International Symposium on Nuclear Physics—Dynamics of Heavy-Ion Collisions, Nov. 10–14, 1986, Gaussig, GDR*, edited by R. Reif and R. Schmidt (ZfK, Rossendorf, GDR, 1986).

[24]L. Vinet, C. Grégoire, P. Schuck, B. Rémaud, and F. Sébille, Nucl. Phys. **A468**, 321 (1987).